H-Type Dimer Formation of Fluorophores: A Mechanism for Activatable, *in Vivo* Optical Molecular Imaging

Mikako Ogawa, Nobuyuki Kosaka, Peter L. Choyke, and Hisataka Kobayashi*

Molecular Imaging Program, Center for Cancer Research, National Cancer Institute, National Institutes of Health, Bethesda, Maryland 20892-1088

Molecular imaging enables the visualization of specific molecules *in vivo*. Molecular probes for *in vivo* imaging typically consist of a targeting ligand, linker molecule, and imaging "beacon" (*1, 2*). Among the imaging beacons, optical fluorescent molecules have the advantages of higher sensitivity and lower cost compared to other imaging modalities but suffer from the well-recognized limitation of poor tissue penetration, which restricts their application to surface or near-surface phenomena. However, a desirable property of fluorescent signals is that they can be "switchable", enabling the development of target-specific activatable "smart" probes that become fluorescent only at the intended target (*1, 3*). Smart probes have the potential to detect pathology *in vivo* with high sensitivity and specificity because background signal is minimized and thus target to background ratios are high. There are a number of mechanisms for generating activatable probes, but all require efficient quenching in the "off" state. These include photon-induced electron transfer (PeT) (*4, 5*) and homo- and heterofluorescence resonance energy transfer (FRET) (*6–8*).

Some fluorophores, such as rhodamine and BODIPY derivatives, form homodimers at relatively high concentrations, and the photophysical chemistry underlying quenching by dimerization in concentrated aqueous solutions has been well studied (*9–12*). This homodimer formation induces short (H-dimer) or long (J-dimer) shifts of absorbance spectra, which completely quench the emission fluorescence signal (*13*). Since the dissociation constants of these dimers are large ($\sim10^{-4}$–10^{-5} M) (*13, 14*), dimer formation of fluorophores alone is not expected to occur at the concentrations (nanomolar to picomolar) typically used for *in vivo* molecular imaging.

ABSTRACT *In vivo* molecular imaging with target-specific activatable "smart" probes, which yield fluorescence only at the intended target, enables sensitive and specific cancer detection. Dimerization and fluorescence quenching has been shown to occur in concentrated aqueous solutions of various fluorophores. Here, we hypothesized that fluorophore dimerization and quenching after conjugation to targeting proteins can occur at low concentration. This dimerization can be exploited as a mechanism for fluorescence activation. Rhodamine derivatives were conjugated to avidin and trastuzumab, which target D-galactose receptor and HER2/neu antigen, respectively. After conjugation, a large proportion of R6G and TAMRA formed H-type dimers, even at low concentrations, but could be fully dequenched upon dissociation of the dimers to monomers. To demonstrate the fluorescence activation effect during *in vivo* fluorescence endoscopic molecular imaging, a highly quenched probe, avidin-TAMRA, or a minimally quenched probe, avidin-Alexa488, was administered into mice with ovarian metastases to the peritoneum. The tumors were clearly visualized with avidin-TAMRA, with low background fluorescence; in contrast, the background fluorescence was high for avidin-Alexa488. Thus, H-dimer formation as a mechanism of fluorescence quenching could be used to develop fluorescence activatable probes for *in vivo* molecular imaging.
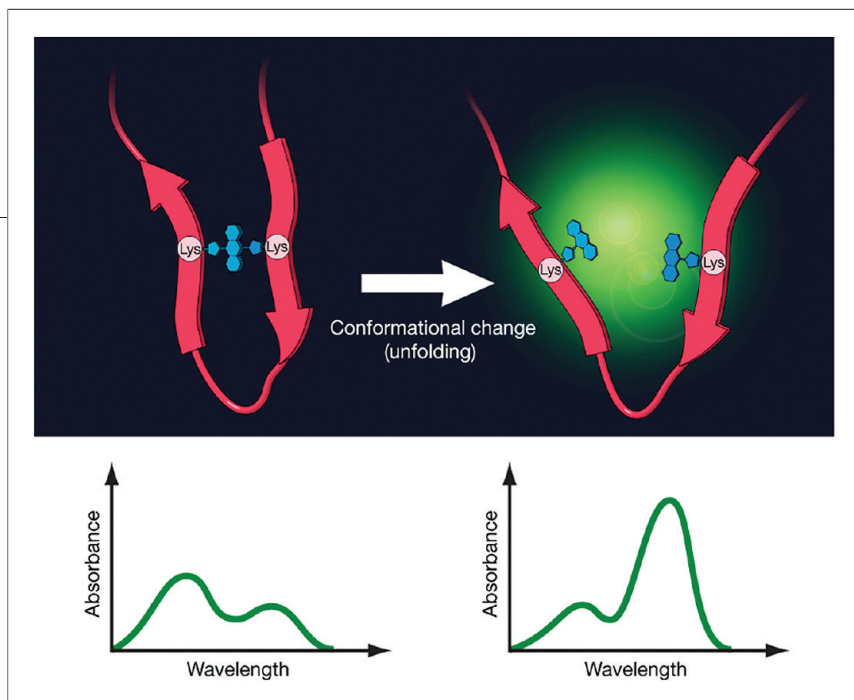
*Corresponding author,
kobayash@mail.nih.gov.

Figure 1. Schema of quenching and activation mechanism employing H-dimer formation after binding to the protein.

However, when target-specific molecular probes are synthesized, fluorophores are covalently conjugated with target-specific proteins such as antibodies or receptor ligands, which have distinct, stable conformations under physiological conditions. Indeed, it is common that a fluorophore produces less light after conjugation with a protein than it does in its pure state (8, 15, 16). We speculated that protein molecules can facilitate H-dimer formation at low fluorophore concentrations, because each fluorophore theoretically has only a few preferential reaction sites on a protein based on physicochemical characteristics such as charge and hydrophilicity. These characteristics might lead to crowding of fluorophores at specific sites on the protein, resulting in homodimer formation and quenching.

Furthermore, we hypothesized that fluorophore dimer formation, after protein binding, is potentially dissociable after conformational change or catabolism of the bound protein resulting in activation of the released fluorophore (Figure 1). In the case of cancer imaging, dimer formation of fluorophores bound to target-specific proteins leads to quenching that is dissociable after internalization and catabolism of the probe within the cell but not outside the cell, leading to high tumor to background ratios (TBRs). In this study, we evaluate the efficacy of various fluorophores (listed in Figure 2) to form homo (H)-dimers on cancer targeting proteins and then demonstrate that efficient H-dimer formation is a practical mechanism to generate activatable optical molecular imaging probes for *in vivo* molecular imaging of cancer.

RESULTS AND DISCUSSION

Mass Spectral Analysis of H-dimer Formed Av-TAMRA. Although the TAMRA–avidin (tetramer) ratio was approximately 3:1, each avidin monomer is frequently conjugated with 2 fluorophores as shown by the mass spectral analysis (Supplementary Figure 2). This data suggests fluorophores tended to cluster in proximate pairs on monomers after conjugation with avidin. In addition, despite random conjugation, we found the lysine residue located at site 90 was a preferential con-
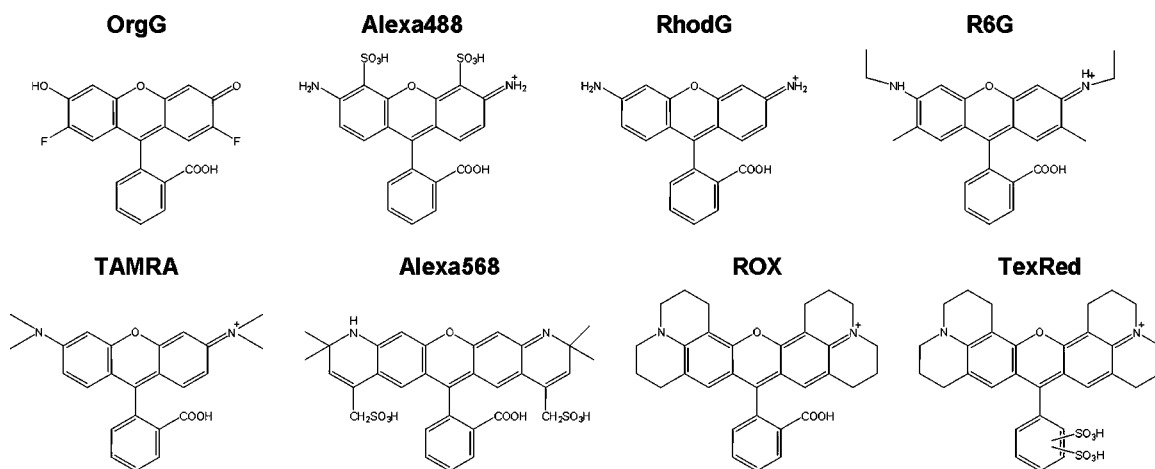
Figure 2. Chemical structures of several rhodamine fluorophores: Oregon Green (OrgG), Alexa Fluor488 (Alexa488), Rhodamine Green (RhodG), Rhodamine 6G (R6G), TAMRA, Alexa Fluor568 (Alexa568), ROX or Texas Red-X (TexRed)
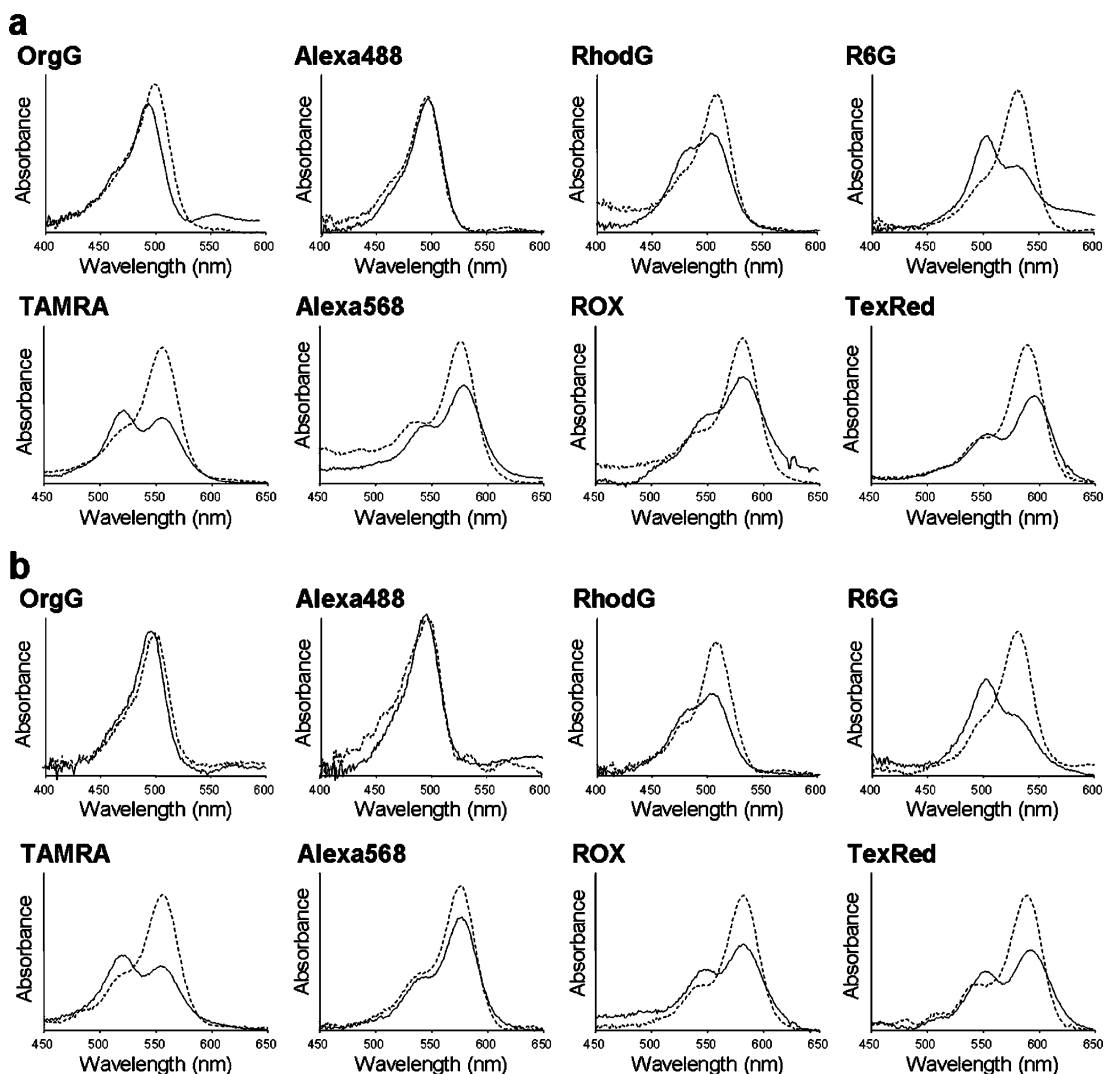
Figure 3. Absorbance spectrum of rhodamine fluorophores without SDS (solid line) and with SDS (dashed line). The blue-shifted peak without SDS represents H-dimer formation of fluorophores. Both avidin (a) and trastuzumab (b) conjugates showed a similar tendency for each fluorophore tested.

jugation site, although we could not determine the full spectrum of conjugation sites on the avidin molecule.

Effect of H-dimer Formation on Absorption Spectrum and Fluorescence Intensity. The dimerization and resulting fluorescence quenching of rhodamine fluorophores in concentrated aqueous solutions are known phenomena in photochemistry (*9–14*). We sought to determine if this concept could be applied to macromolecular conjugation chemistry in the design of targeted activatable fluorescent probes for *in vivo* molecular im-

aging. The fluorophores were conjugated to a cancer targeting molecule, avidin, and a humanized monoclonal antibody, trastuzumab, which bind D-galactose receptor and human epidermal growth factor receptor type 2 (HER2/*neu*) antigen, respectively.

The absorption spectra of each conjugate without (solid lines) and with (dashed lines) SDS-induced unfolding are shown in Figure 3. Without SDS, the spectra showed H-dimer formation with the appearance of a blue-shifted peak (except for OrgG and Alexa488) in

TABLE 1. H-dimer extents and fluorescence quenching capacities of avidin or trastuzumab-rhodamine conjugates

	Avidin conjugates		Trastuzumab conjugates	
	H-dimer extent	Quenching capacity	H-dimer extent	Quenching capacity
OregG	0.86	2.6	0.97	1.1
Alexa488	0.69	2.7	0.91	1.0
RhodG	1.70	2.5	1.89	3.7
R6G	3.58	13.5	3.63	8.9
TAMRA	2.74	10.0	2.79	7.4
Alexa568	1.41	3.1	1.16	1.9
ROX	1.72	4.1	2.13	7.2
TexRed	1.67	10.1	2.00	12.0

both avidin and trastuzumab conjugates. J-Dimer was not observed with any fluorophore. With SDS, the H-dimers were separated into monomers and H-dimer formation could be expressed as

$$\text{H-dimer extent} = \frac{(A_{di}\ w/o\ SDS)/(A_{mo}\ w/o\ SDS)}{(A_{di}\ in\ SDS)/(A_{mo}\ in\ SDS)}$$

(1)

Here, A_{di} and A_{mo} represent the absorbance at the H-dimer peak and at the monomer peak, respectively. The results are summarized in Table 1. The changes in fluorescence intensity after SDS administration, that is, the quenching capacities, are also shown in Table 1. The strongest fluorescence activation or quenching capacity was seen for TAMRA, R6G, and TexRed in both avidin and trastuzumab conjugates. It is well-known that pyrenes form excimers at high concentration and emit longer and broader wavelength fluorescence than do monomers, because of complex ground state and excited state molecules (17). This is a useful characteristic for making molecular beacons for *in vitro* studies (18). In this study, we could not detect excimer formation on the basis of the specific shape of the emission profile of all rhodamine-based probes tested in this study.

The correlation between the extent of H-dimer formation and fluorescence quenching efficiency is plotted in Figure 4, panels a and b and shows a strong positive relationship in both avidin and trastuzumab conjugates

($r = 0.86$ for avidin, $r = 0.74$ for trastuzumab). The one exception was TexRed conjugated proteins, which showed a lower dimerization rate despite high quenching efficiency. This might be explained by the overlapping involvement of other fluorescence quenching mechanisms such as fluorescence resonance energy transfer (FRET) between fluorophores. To clarify the contribution of the non-absorbance shifted fraction, which represents the monomer form, in fluorescence quenching (mainly FRET), we calculated that fraction on the basis of the difference in absorbance value and fluorescence yield at the monomer wavelength with and without SDS. As shown in Table 2, longer emission wavelength fluorophores tend to have a larger proportion of FRET-induced quenching that contributed to increasing the quenching capacity for ROX and TexRed. In addition, there were good relationships between the reaction ratio (TAMRA and trastuzumab), quenching efficiency, and H-dimer formation (Figure 5). This suggests that the higher fluorophore to protein ratios are more likely to form H-dimer; however, too much fluorophore on one targeting protein might lead to a decrease in binding affinity with the targeting molecule.

To confirm the effect of H-dimer formation on fluorescence emission, fluorescence intensities were measured at both H-dimer and monomer absorption peaks for Av-R6G and Av-TAMRA. The fluorescence intensity was higher when the conjugates were excited at the monomer peak than when excited at the H-dimer peak whether or not they were treated with SDS (Figure 6). The intensity ratios (monomer/dimer) were almost the same with or without SDS (ratio = 2 for Av-R6G and ratio = 3 for Av-TAMRA), that is, fluorescence was proportionally increased when excited at the monomer peak regardless of the degree of H-dimer formation. These results support the concept that dimerized fluorophores conjugated to proteins are minimally fluorescent.

Then, the log P values of each fluorophore molecule were measured to investigate the effect of lipophilicity on H-dimer formation (Table 3). The lipophilicity was highest in ROX and lowest in Alexa488. There was a correlation between lipophilicity and the degree of H-dimer formation (Figure 4, panels c and d; $r = 0.66$ for avidin, $r = 0.75$ for trastuzumab). This indicates that lipophilicity is one of the causes of H-dimer formation within these probes. Hydrophilicity shows moderate correlation with HOMO values of the free dyes calculated with the B3LYP/6-31G method, which however might be
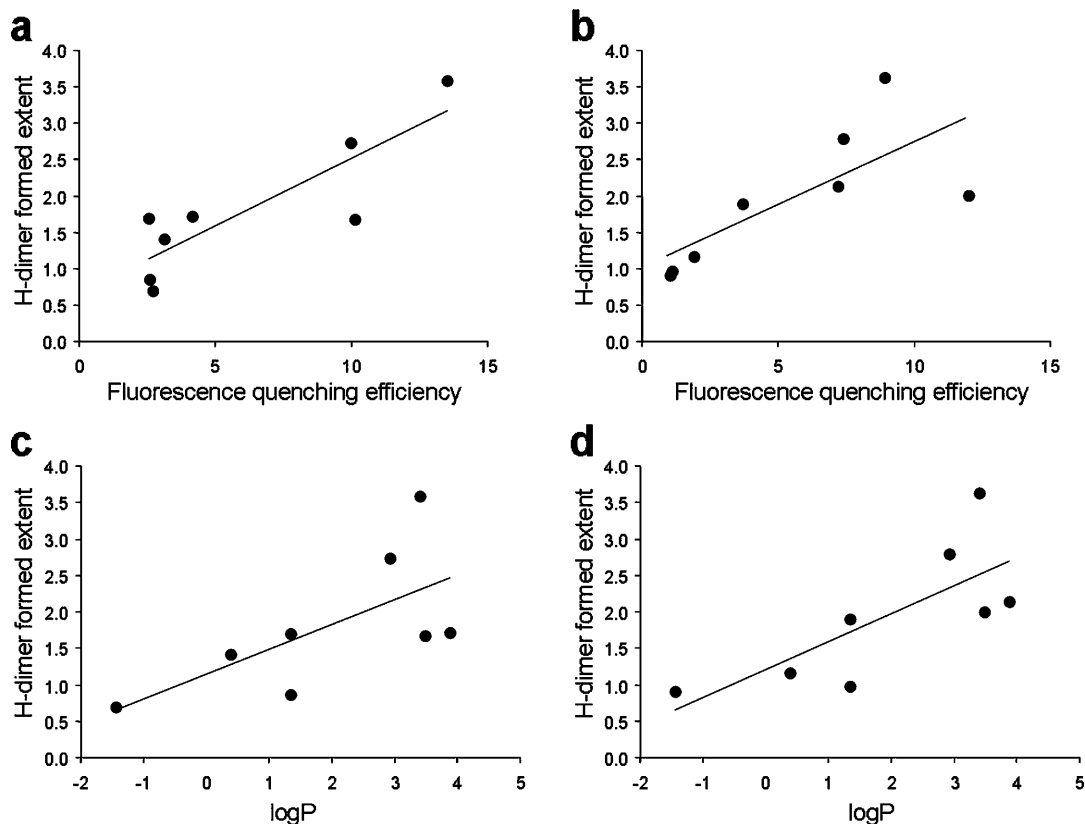
Figure 4. Correlation between fluorescence quenching efficiency and H-dimer formation (a, b), and fluorophore lipophilicity (log *P*) and H-dimer formation (c, d) for various rhodamine-avidin (a, c) and rhodamine-trastuzumab conjugates (b, d). Strong correlation was observed between H-dimer formation and fluorescence quenching. A relationship was also found between lipophilicity and H-dimer formation. This indicates that fluorophore lipophilicity is one of the causes for H-dimer formation on the protein molecule.

TABLE 2. Extents of FRET contribution in fluorescence quenching

	FRET (%)	Quenching capacity (by FRET)[a]
OregG	<0	<0
Alexa488	<0	<0
RhodG	45.8	1.8
R6G	<0	<0
TAMRA	14.5	1.1
Alexa568	32.9	0.6
ROX	60.9	4.4
TexRed	78.1	9.3

[a]Data were calculated by (quenching capacity in Table 1) × (FRET (%))/100.

altered after conjugation with protein. Therefore, other chemical characteristics (e.g., HOMO/LUMO and charge distribution) in the conjugates might also affect H-dimer formation. Furthermore, the interaction between the fluorophores and generic aromatic amino acids in targeting proteins might provide additional quenching effects. Despite very different conformational and chemical characteristics of the two targeting ligands, only slight differences in H-dimer formation were observed between avidin and trastuzumab conjugated with the same fluorophore. This slight difference between avidin and trastuzumab might derive from this fluorophore–protein interaction.

Interestingly, H-dimers were formed at lower fluorophore concentrations than has been reported previously with free fluorophores. The dissociation constant
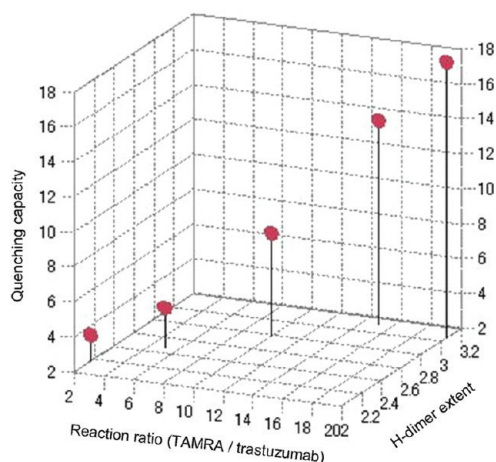
Figure 5. Relationships between the reaction ratio, quenching efficiency, and H-dimer formation in trastuzumab-TAMRA conjugates. A higher labeling density per target molecule (called reaction ratio) correlated well with a higher quenching capacity (called quenching efficiency) and shorter absorbance shift (H-dimer formation). Good relationships were observed in these three parameters.

of R6G H-dimer was reported to be 590 μM (*14*). The fluorophore concentrations after protein conjugation used in this study were 0.22 and 0.10 μM (absorbance), and 0.11 and 0.10 μM (fluorescence) for avidin and trastuzumab, respectively. These results support the hypothesis that the protein molecules can promote and stabi-

lize H-dimer formation for rhodamine fluorophores. The practical implication of these results is that H-dimer formation in molecular imaging probes can behave as "activatable probes" for *in vivo* imaging because the quenching is stable even after dilution in the body circulation and can be retained until the probes bind to the target, internalize, and are catabolized in the lysosome.

***In Vitro* Fluorescent Microscopy Studies in Cancer Cells.** In order to demonstrate the system in cancer cells, *in vitro* cell experiments were performed using fluorescence microscopy. Both trastuzumab-TAMRA and trastuzumab-Alexa488 showed fluorescent signal on the surface of 3T3/HER2+ cells with 8 h 4 °C incubation, trastuzumab-Alexa488 resulting in somewhat

a

b
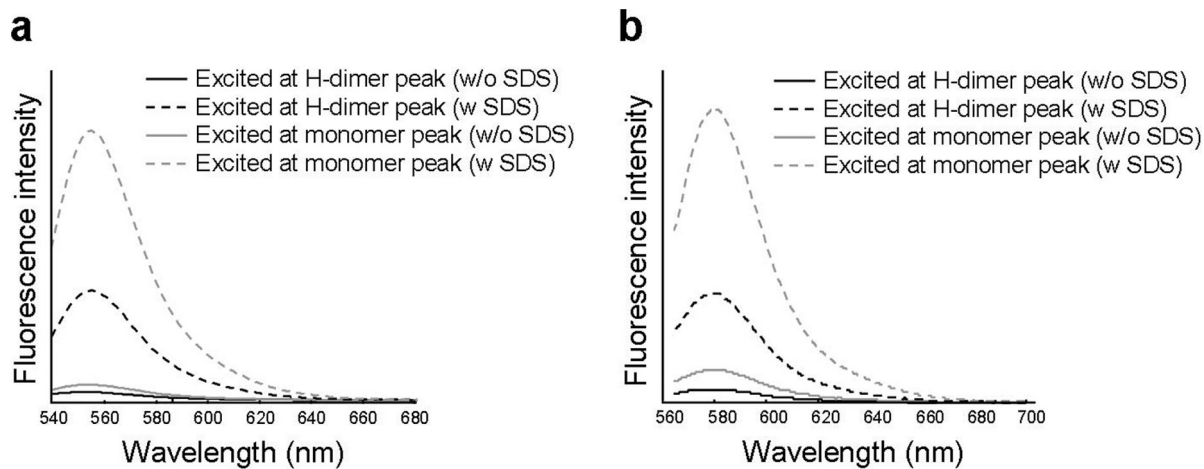
Figure 6. Fluorescence spectra of Av-TAMRA (a) and Av-Alexa488 (b). The conjugates were excited at either the dimer peak (black line) or the monomer peak (gray line) without SDS (solid line) and with SDS (dashed line). The fluorescence intensity was higher with the monomer peak excitation than with the dimer peak excitation with and without SDS. This indicates less H-dimer formation with these conjugates.
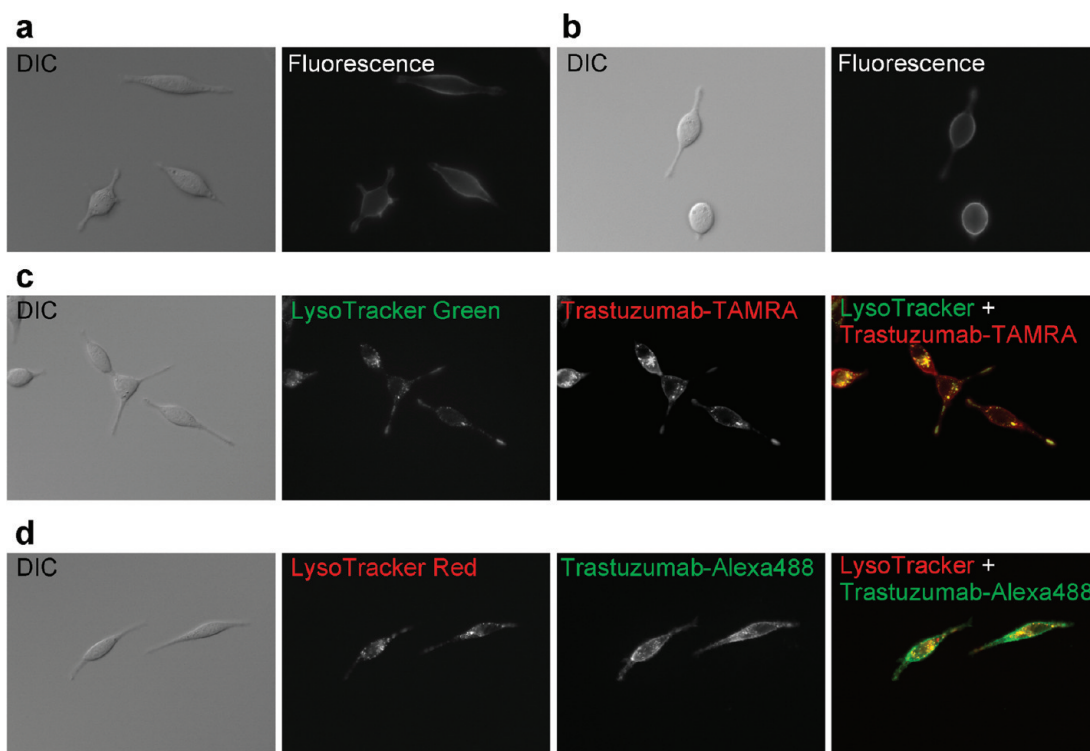
Figure 7. Fluorescence microscopy and differential interference contrast (DIC) images in 3T3/HER2+ tumor cells. Trastuzumab-TAMRA (a) and trastuzumab-Alexa488 (b) showed fluorescent signal on the surface after 8 h of incubation at 4 °C. Fluorescent dots were detected within the cytoplasm after 8 h of incubation at 37 °C with both conjugates (trastuzumab-TAMRA (c), trastuzumab-Alexa488 (d)), and temperature-dependent internalization was observed. The fluorescent dots from TAMRA and Alexa488 were matched with lysosomal marker fluorescence.

brighter signal (Figure 7, panels a and b). Fluorescence was observed inside the cell after 8hrs of incubation at 37 °C with both conjugates, and the intracellular fluorescent dots were brighter with trastuzumab-TAMRA (Figure 7, panels c and d). This observation shows the fluorescence activation after the temperature-dependent internalization for trastuzumab-TAMRA, which has higher quenching efficiency. In addition, the fluorescent dots were co-localized to the lysosome marker for both conjugates (Figure 7, panels c and d). These data supported our hypothesis that both trastuzumab-Alexa488 and trastuzumab-TAMRA bound to the cell surface receptor, were then internalized into the cells, and then could be denatured in the endolysosomes.

In Vitro Receptor Blocking Studies. The receptor blocking experiments were performed to investigate whether the binding of Av-TAMRA and subsequent fluorescence activation is receptor-dependent. As shown in

Figure 8, panel a, fluorescence accumulation in SHIN3 cells was blocked by GSA treatment. FACS flow cytometry results are shown in Figure 8, panel b. The mean values were 1.6, 10.9, and 2.6 for control, Av-TAMRA, and Av-TAMRA+GSA, respectively. These observations show that the internalization and fluorescence activation of Av-TAMRA is mediated by the D-galactose receptor.

***In Vivo* Fluorescence Endoscopy and *in Situ* Fluorescence Spectral Imaging of Tumor Implants.** To demonstrate the fluorescence activation effect of H-dimer formed molecular target probes during *in vivo* molecular imaging of tumor implants, fluorescence endoscopy was performed using the highly quenched probe, Av-TAMRA, and the minimally quenched probe, Av-Alexa488 (Figure 9, panels a and b). The tumors were visualized with Av-TAMRA, with low background fluorescence indicating dequenching primarily within the targeted tumors. In contrast, the background fluorescent signal was high for Av-Alexa488. The calculated TBRs
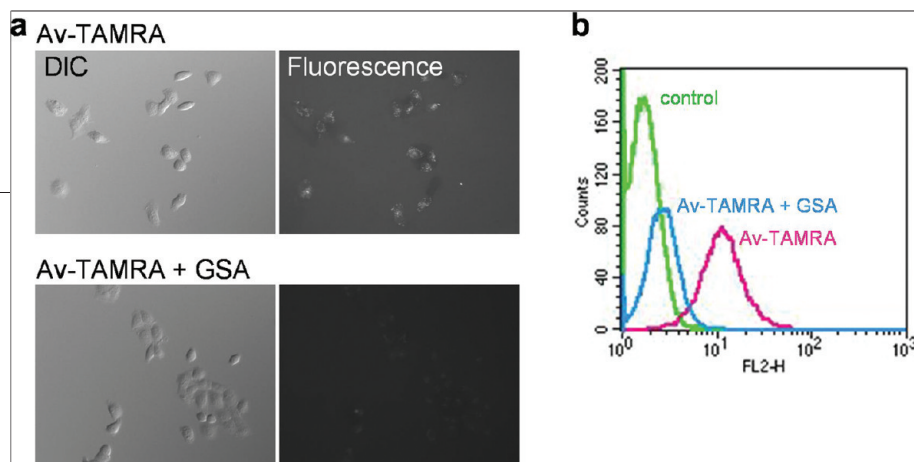
Figure 8. Results of *in vitro* blocking studies in SHIN3 cells. Fluorescence microcopy shows a decrease in Av-TAMRA accumulation within cells after blocking with the unlabled ᴅ-galactose receptor ligand GSA (a). FACS flow cytometry results are shown in panel b. The fluorescence accumulation of Av-TAMRA was blocked by GSA. This suggests that the internalization and subsequent fluorescence activation of Av-TAMRA arises from the ᴅ-galactose receptor mediated pathway.

were 23.3 ± 14.1 and 1.8 ± 0.5 for Av-TAMRA and Av-Alexa488, respectively, a statistically significant difference ($P < 0.0001$, Mann−Whitney *U*-test, Figure 9, panel c). To validate the *in vivo* results, we performed tissue biopsy under fluorescence guided endoscopy with trastuzumab-TAMRA. The sampled tissues ($n = 50$; 25 from fluorescent tissue, 25 from nonfluorescent tissue) were histologically analyzed and demonstrated perfect sensitivity/specificity for tumor/nontumor (100/100%).

After the endoscopic imaging, fluorescence spectral imaging was performed. Again, the tumor nodules were clearly imaged by Av-TAMRA with fairly low background signal; in contrast, the background signal was high for Av-Alexa488 (Figure 9, panels d and e). The results corroborated the *in vivo* endoscopic images. Such high target to background fluorescence ratios lead to improved detection of small cancers. Ideally, high target to background ratios are achieved by minimizing signal from nontumor tissue while maximizing signal from target tumor cells. This can be achieved by switching on the fluorophore only once it is inside the target cell. H-dimer formation results in high TBRs, so that Av-TAMRA H-dimers depicted tiny cancer nodules clearly with low background signal (Figure 8, panels b and e). In contrast, the nondimerized, "always on" probe, Av-Alexa488, showed high background fluorescence making detection of all but the largest tumors quite difficult (Figure 9, panels a and d). These observations are consistent with a previous study in which several rhodamine fluorophores were conjugated to a tumor targeting molecule, galactosyl serum albumin, and investigated both *in vitro* and *in vivo* (19). Among the rhodamine fluorophores used, TAMRA had the best fluorescent properties as an *in vivo* molecular imaging probe.

Effective activatable optical probes can be designed by focusing on the chemical features of fluorophores that are predisposed to H-dimer formation. Furthermore, the concept of dimerization may be applicable to intermolecular interactions between different molecules, such as fluorophore-quencher pairs. For instance, TAMRA and QSY7 are an efficient quenching-dequenching pair, which likely suppress emission by a combination of hetero-FRET effects and H-dimer formation (7). Although we successfully synthesized activatable imaging probes with a TAMRA and QSY7 fluorophore-quencher pair, 11 other fluorophore-quencher pairs, which were thought to be appropriate FRET pairs, were found to produce only "always on" or even "always off" imaging probes (20). Thus, there are only a limited number of successful fluorophore-quencher combinations, which limits the applicability of this method. Additionally, it is thought that fluorophore-quencher combinations form significant amounts of both hetero and homo H-dimers after conjugating to protein, whereas the H-dimer mechanism is based on homo dimer formation. We acknowledge that it is difficult to actually determine the amount of hetero dimer formation. In contrast to fluorophore-quencher combinations, most of the H-dimer-forming rhodamine-derivative conjugates that we tested were successful as target cell-specific activatable probes with the exception of TexRed. Therefore, unlike the fluorophore-quencher strategy, which is quite unpredictable, quenched targeted reagents based on H-dimer formation reliably activated in accordance with the amount of H-dimer present as determined by absorbance. Thus, probes based on H-dimer quenching are likely to be more generalizable than fluorophore-quencher combinations. Since these different quenching mechanisms can operate independently, it may be possible to design probes based on the combinational use of more than one mechanism including PeT, FRET, and H-dimer, to develop even more effective activatable molecular imaging probes.
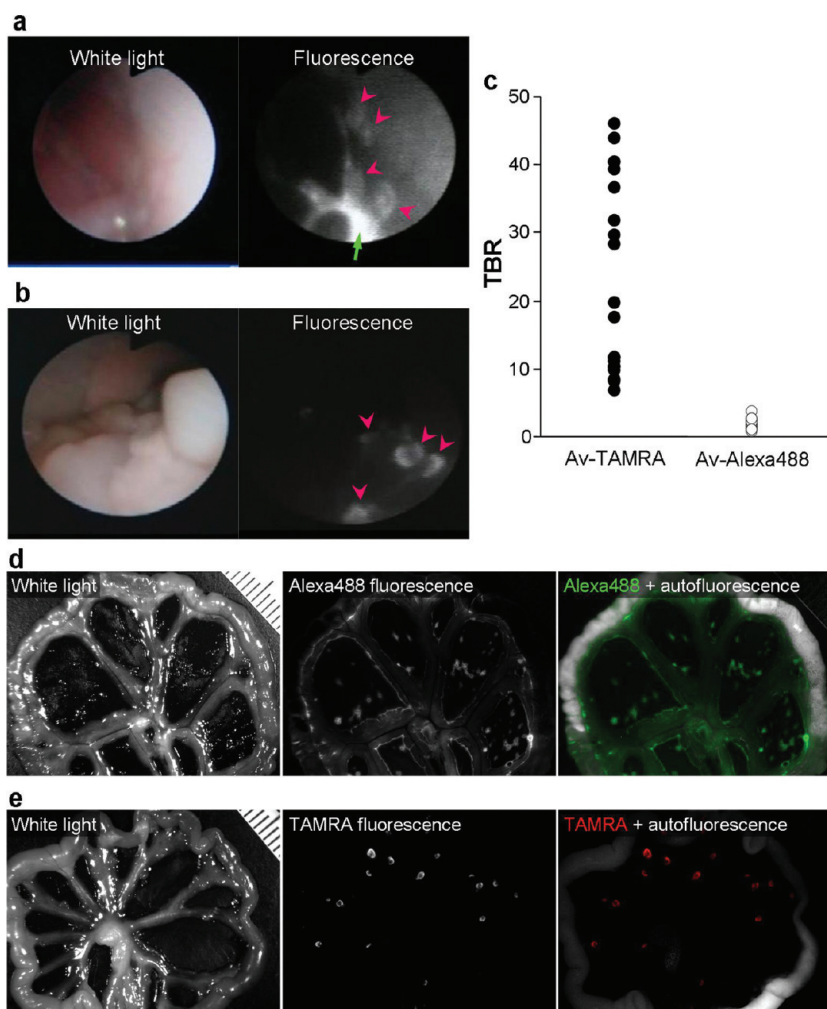
Figure 9. *In vivo* fluorescence endoscopic images in tumor-bearing mice enhanced by Av-Alexa488 (a) and Av-TAMRA (b). The pink arrow heads show the tumor nodules. The tumors were clearly visualized with the activatable probe Av-TAMRA. In contrast, Av-Alexa488, an always-on probe, showed high background signal and high fluorescence from excess inject-ate in the peritoneal cavity (green arrow). The measured TBR was higher for Av-TAMRA than for Av-Alexa488 (c). Fluorescence spectral images of the peritoneal membranes for Av-Alexa488 (d) and Av-TAMRA (e). The results were consistent with endoscopic images. Tumors were detected with low background signal for Av-TAMRA, but the background was high for Av-Alexa488.

lipase A2 (PLA2) activities *in vivo* in zebrafish (*22, 23*). They employed BODIPY and a quencher and combined them with phospholipid substrate analogues. This probe showed better quenching and de-quenching (activation) efficacy than our macro-molecular probes based on quencher-fluorophore pairs (*7*). These small molecular imaging probes generally produced specificity by cleavage with a specific enzyme. From a chemistry perspective, these probes can be perfectly designed and synthesized, to amplify the signal from a single enzyme molecule. However, from a biological perspective, there are very few enzymes specifically expressed in cancer cells that are not also expressed in normal cells and tissues. The strategy for targeting cell surface molecules can produce better specificity; however, this can be successfully achieved only with targeted macromolecules including antibodies or receptor ligands. Therefore, although the chemical function or purity in macromolecular probes is not as good as that of small molecular probes, macromolecular probes might have the advantage of biological specificity in molecular imaging probes for cancer (*5*).

Optical imaging represents a powerful technology especially for cancer research. Currently, *in vivo* imag-

It should be noted that there are already a number of targeted, activatable small molecule probes. Jiang *et al.*, for instance, synthesized molecular probes that bind to the cell in the presence of specific cleaved enzymes which could be useful for *in vivo* molecular imaging (*21*). Hendrickson *et al.* successfully synthesized an intramolecularly quenched probe to image phospho-

ing applications include (i) the study of cancer biology *in vivo* through expression and imaging of endogenously expressed fluorescent proteins and (ii) the development of clinical applications for guiding the diagnosis/treatment of cancer with disease-specific fluorescent probes. Early studies involving imaging of fluorescent proteins revealed the potential of optical imaging in cancer biology, such as for the repeated imaging of cancer invasion and metastasis in longitudinal studies (*24*). One limitation to the use of fluorescent proteins for cell labeling in humans is that this process necessitates gene transfection, which may present problems for clinical imaging (*25*). Injectable fluorescent molecules chemically conjugated with or-

ganic fluorophores, however, are well-suited to the development of optical probes for clinical applications as they do not require manipulation of the host genome.

In conclusion, we demonstrate that H-dimer formation derived fluorescence quenching occurs when fluorophores are conjugated to some proteins, which in the case of molecular imaging probes may be targeting ligands. After internalization and dissociation of the H-dimer in the target cell, dequenching occurs, permitting high target to background imaging. Thus, H-dimer formation is a promising mechanism for activation of target-specific macromolecular optical probes for molecular imaging.

METHODS

Reagents. The NHS esters of Oregon Green (OrgG), Alexa Fluor488 (Alexa488), Rhodamine Green (RhodG), Rhodamine 6G (R6G), TAMRA, Alexa Fluor568 (Alexa568), ROX, and Texas Red-X (TexRed) were purchased from Invitrogen Corporation (Carlsbad, CA). Avidin was purchased from Pierce Biochemical, Inc. (Milwaukee, WI). Trastuzumab, an FDA-approved humanized anti-HER-2 antibody, was purchased from Genentech Inc. (South San Francisco, CA). All other chemicals used were of reagent grade.

Synthesis of Fluorophore-Conjugated Avidin and Trastuzumab. Two proteins, avidin (targeting D-galactose receptor) and trastuzumab (a humanized monoclonal antibody against the human epithelial growth factor receptor type2 (HER2/neu) were selected as tumor targeting agents.

Avidin (14 nmol) was incubated with NHS esters of OrgG, Alexa488, RhodG, R6G, TAMRA, Alexa568, ROX, and TexRed (70 nmol) in 0.1 M Na_2HPO_4 (pH 8.5) at RT for 30 min. Each mixture was purified with a Sephadex G50 column (PD-10; GE Healthcare, Piscataway, NJ). For antibody conjugates, trastuzumab (6.5 nmol) was treated with NHS esters (65 nmol) and purified in the same manner as above. The number of fluorophore molecules per trastuzumab was approximately 3.

Measurement of Absorption Spectrum of the Synthesized Conjugates. The absorption spectrum was measured with UV–vis system (8453 Value UV–visible Value System; Agilent Technologies, Santa Clara, CA) by diluting the resulting solution to 73.6 and 34.3 nM as protein concentrations for avidin and trastuzumab conjugates, respectively. The concentrations, which were calculated on the basis of fluorophores, were 0.22 and 0.10 μM for avidin and trastuzumab conjugates, respectively.

To dissociate the dimerized fluorophores, SDS (5%) was added to the solution, and the absorption spectrum was measured and compared to non-SDS-treated solutions at the same concentrations.

Fluorescent Intensity Measurements. The fluorescence intensity was measured with a fluorescence spectrometer (Perkin-Elmer LS55, Perkin-Elmer, Shelton, CT) both without and with SDS at concentrations of 36.8 and 34.3 nM, for avidin and trastuzumab conjugates, respectively. The concentrations calculated on the basis of fluorophores were 0.11 and 0.10 μM for avidin and trastuzumab conjugates, respectively. The excitation wavelength used was based on the intrinsic absorption maximum for each fluorophore in its monomeric form.

The non-absorbance shifted fraction, which represents the existence of monomer (mainly FRET fraction), in fluorescence quenching was estimated by the following equation, where *A* or *B* is a fluorescence intensity without or with SDS, at the same monomer absorbance value: FRET % = $(A - B)/B$.

To eliminate the dimer contribution from the monomer absorbance, we used the linear approximation at the overlapping spectra to adjust the baseline and obtained the area underneath the curve.

For the H-dimer conjugates, Av-R6G and Av-TAMRA, the fluorescence intensities were also measured at a blue-shifted peak (H-dimer peak) and intrinsic absorption maxima (monomer peak) with and without SDS to investigate the effect of H-dimer formation on fluorescence emission.

Estimation of log *P* Value of Each Fluorophore Molecule. The estimates of the logarithm of partition coefficient in *n*-octanol/water (log *P*) were obtained by use of Crippen's fragmentation method (*26*).

Fluorescence Microscopy Studies with Antibody Conjugates. 3T3/HER2+ cells (1×10^4) were plated on a cover glass-bottomed culture well and incubated for 16 h. Then, trastuzumab-TAMRA or trastuzumab-Alexa488 was added to the medium (30 μg mL^{-1}), and the cells were incubated for 8 h either on ice or at 37 °C. After incubation, cells were washed once with PBS, and fluorescence microscopy was performed using an Olympus BX51 microscope (Olympus America, Inc., Melville, NY) equipped with the following filters: green filter sets were used for TAMRA fluorescence (excitation wavelength 530−585 nm, emission wavelength 605−680 nm), and blue filter sets were used for Alexa488 fluorescence (excitation 470−490 nm, emission wavelength 515−550 nm). Transmitted light differential interference contrast images were also acquired. To investigate the intracellular localization of the conjugates, co-localization studies were performed using a lysosomal marker (LysoTracker Green for trastuzumab-TAMRA or Lyso-Tracker RED for trastuzumab-Alexa488, Invitrogen Co.). Lyso-Tracker was added 30 min prior to imaging. The blue or green filter sets were additionally employed for LysoTracker Green or LysoTracker RED, respectively.

***In Vitro* Receptor Blocking Studies.** To investigate receptor specificity, *in vitro* blocking studies were performed. SHIN3 cells (1×10^4) were plated on a cover glass-bottomed culture well and incubated for 16 h. Av-TAMRA was added to the medium (3 μg mL^{-1}), and the cells were incubated for 8 h at 37 °C.

After incubation, cells were washed once with PBS, and fluorescence microscopy was performed as described above with the green filter sets. For the blocking study, the D-galactose receptor ligand, galactosyl serum albumin (GSA, 30 μg mL^{-1}) was added to the medium.

One-color flow cytometry studies were also performed. SHIN3 cells were placed on a 12-chamber well and incubated for 16 h. Av-TAMRA was added to the medium (10 μg mL^{-1}) and cells were incubated for 12 h at 37 °C. GSA (100 μg mL^{-1}) was also added to the medium for blocking. After the incubation, the cells were washed with ice-cold PBS, and flow cytometry was performed employing 488 nm laser for excitation. Signals from cells were collected using 585/42 nm band-pass filter.

***In Vivo* Fluorescence Imaging in Mice Bearing Peritoneal Tumors.** All procedures were carried out in compliance with the Guide for the Care and Use of Laboratory Animal Resources (1996), National Research Council and approved by the National Cancer Institute Animal Care and Use Committee. Intraperitoneal (i.p.) tumor implants were introduced by an i.p. injection of 2×10^6 SHIN3 (D-galactose receptor positive ovarian cancer cells) in female nude mice (National Cancer Institute Animal Production Facility, Frederick, MD). The imaging studies were performed 3 weeks after the injection of tumor cells. Alexa488 conjugated avidin (Av-Alexa488) or TAMRA conjugated avidin (Av-TAMRA) was injected into the SHIN3 peritoneal tumor bearing mice (50 μg, i.p., $n = 3$). These probes were tested in live animals after i.p injection of the probes into the abdomen of mice with peritoneal dissemination of ovarian cancer. Intraperitoneal dosing was less likely to be affected by pharmacokinetics than intravenously injected molecular probes. Two hours after the conjugates were injected, the mice were anesthetized with pentobarbital (30 mg kg^{-1} i.v., with 0.1% scopolamine butyl bromide), and fluorescence endoscopy was performed using the Olympus EVIS ExERA-II CLV-180 system (Olympus Corp., Tokyo, Japan). The excitation wavelengths used were 482/35 nm and 543/25 nm for Av-Alexa488 and Av-TAMRA, respectively. The emission filters were 536/40 nm and 597.5/55 nm for Av-Alexa488 and Av-TAMRA, respectively. The fluorescence intensities of tumor and background were measured on the images ($n = 20$) using Image-J software (National Institutes of Health, Bethesda, MD, http://rsb.info.nih.gov/ij/), and the TBR was calculated. In addition, we performed tissue biopsy from 50 sites with or without fluorescence signal (25 in each) under fluorescence guided endoscopy (as shown in Supplementary Video C). The tissues were embedded in paraffin and stained with H&E.

After endoscopy, the mice were sacrificed with carbon dioxide and *ex vivo* imaging of the peritoneal implants was performed on a Maestro In-Vivo Imaging System (CRi, Inc., Woburn, MA). A band-pass excitation filter from 445 to 490 nm and a long-pass emission filter over 515 nm were used for detecting Alexa488 fluorescence, and a band-pass excitation filter from 503 to 555 nm and a long-pass emission filter over 580 nm were used for detecting TAMRA fluorescence. The tunable emission filter was automatically stepped in 10-nm increments from 500 to 800 nm while the camera captured images at each wavelength interval with constant exposure. The spectral fluorescence images consisting of autofluorescence spectra and the spectra from Alexa488 or TAMRA were obtained and then unmixed on the basis of their spectral patterns.

Supporting Information Available: This material is available free of charge *via* the Internet at http://pubs.acs.org.

REFERENCES

1. Weissleder, R., and Mahmood, U. (2001) Molecular imaging, *Radiology 219*, 316–333.
2. Weissleder, R., and Pittet, M. J. (2008) Imaging in the era of molecular oncology, *Nature 452*, 580–589.
3. Urano, Y. (2008) Sensitive and selective tumor imaging with novel and highly activatable fluorescence probes, *Anal. Sci. 24*, 51–53.
4. Kamiya, M., Kobayashi, H., Hama, Y., Koyama, Y., Bernardo, M., Nagano, T., Choyke, P. L., and Urano, Y. (2007) An enzymatically activated fluorescence probe for targeted tumor imaging, *J. Am. Chem. Soc. 129*, 3918–3929.
5. Urano, Y., Asanuma, D., Hama, Y., Koyama, Y., Barrett, T., Kamiya, M., Nagano, T., Watanabe, T., Hasegawa, A., Choyke, P. L., and Kobayashi, H. (2009) Selective molecular imaging of viable cancer cells with pH-activatable fluorescence probes, *Nat. Med. 15*, 104–109.
6. Hama, Y., Urano, Y., Koyama, Y., Gunn, A. J., Choyke, P. L., and Kobayashi, H. (2007) A self-quenched galactosamine-serum albumin-rhodamineX conjugate: a "smart" fluorescent molecular imaging probe synthesized with clinically applicable material for detecting peritoneal ovarian cancer metastases, *Clin. Cancer Res. 13*, 6335–6343.
7. Ogawa, M., Kosaka, N., Longmire, M. R., Urano, Y., Choyke, P. L., and Kobayashi, H. (2009) Fluorophore-quencher based activatable targeted optical probes for detecting *in vivo* cancer metastases, *Mol. Pharm. 6*, 386–395.
8. Ogawa, M., Regino, C. A., Choyke, P. L., and Kobayashi, H. (2009) *In vivo* target-specific activatable near-infrared optical labeling of humanized monoclonal antibodies, *Mol. Cancer Ther. 8*, 232–239.
9. Lopez Arbeloa, I., and Ruiz Ojeda, P. (1982) Dimeric states of rhodamine B, *Chem. Phys. Lett. 87*, 556–560.
10. Kemnitz, K., and Yoshihara, K. (1991) Entropy-driven dimerization of xanthene dyes in nonpolar solution and temperature-dependent fluorescence decay of dimers, *J. Phys. Chem. 95*, 6095–6104.
11. Bergstrom, F., Mikhalyov, I., Hagglof, P., Wortmann, R., Ny, T., and Johansson, L. B. (2002) Dimers of dipyrrometheneboron difluoride (BODIPY) with light spectroscopic applications in chemistry and biology, *J. Am. Chem. Soc. 124*, 196–204.
12. Tleugabulova, D., Zhang, Z., and Brennan, J. D. (2002) Characterization of BODIPY dimers formed in a molecularly confined environment, *J. Phys. Chem. B 106*, 13133–13138.
13. Valdes-Aguilera, O., and Neckers, D. C. (1989) Aggregation phenomena in xanthene dyes, *Acc. Chem. Res. 22*, 171–177.
14. Selwyn, J. E., and Steinfeld, J. I. (1972) Aggregation of equilibriums of xanthene dyes, *J. Phys. Chem. 76*, 762–774.
15. Hama, Y., Urano, Y., Koyama, Y., Kamiya, M., Bernardo, M., Paik, R. S., Shin, I. S., Paik, C. H., Choyke, P. L., and Kobayashi, H. (2007) A target cell-specific activatable fluorescence probe for *in vivo* molecular imaging of cancer based on a self-quenched avidin-rhodamine conjugate, *Cancer Res. 67*, 2791–2799.
16. Ogawa, M., Kosaka, N., Choyke, P. L., and Kobayashi, H. (2009) *In vivo* molecular imaging of cancer with a quenching near-infrared fluorescent probe using conjugates of monoclonal antibodies and indocyanine green, *Cancer Res. 69*, 1268–1272.
17. Winnik, F. M. (1993) Photophysics of preassociated pyrenes in aqueous polymer solutions and in other organized media, *Chem. Rev. 93*, 587–614.
18. Fujimoto, K., Shimizu, H., and Inouye, M. (2004) Unambiguous detection of target DNAs by excimer-monomer switching molecular beacons, *J. Org. Chem. 69*, 3271–3275.

19. Longmire, M. R., Ogawa, M., Hama, Y., Kosaka, N., Regino, C. A., Choyke, P. L., and Kobayashi, H. (2008) Determination of optimal rhodamine fluorophore for *in vivo* optical imaging, *Bioconjugate Chem. 19*, 1735–1742.

20. Ogawa, M., Kosaka, N., Urano, Y., Choyke, P. L., and Kobayashi, H. (2009) Activatable optical imaging probes with various fluorophore-quencher combinations, *Progress in Biomedical Optics and Imaging 10 (SPIE Proceedings)* 71900Z-1–71900Z-8.

21. Jiang, T., Olson, E. S., Nguyen, Q. T., Roy, M., Jennings, P. A., and Tsien, R. Y. (2004) Tumor imaging by means of proteolytic activation of cell-penetrating peptides, *Proc. Natl. Acad. Sci. U.S.A. 101*, 17867–17872.

22. Hendrickson, H. S., Hendrickson, E. K., Johnson, I. D., and Farber, S. A. (1999) Intramolecularly quenched BODIPY-labeled phospholipid analogs in phospholipase A(2) and platelet-activating factor acetylhydrolase assays and *in vivo* fluorescence imaging, *Anal. Biochem. 276*, 27–35.

23. Farber, S. A., Pack, M., Ho, S. Y., Johnson, I. D., Wagner, D. S., Dosch, R., Mullins, M. C., Hendrickson, H. S., Hendrickson, E. K., and Halpern, M. E. (2001) Genetic analysis of digestive physiology using fluorescent phospholipid reporters, *Science 292*, 1385–1388.

24. Hoffman, R. M. (2005) The multiple uses of fluorescent proteins to visualize cancer *in vivo*, *Nat. Rev. Cancer 5*, 796–806.

25. Kishimoto, H., Kojima, T., Watanabe, Y., Kagawa, S., Fujiwara, T., Uno, F., Teraishi, F., Kyo, S., Mizuguchi, H., Hashimoto, Y., Urata, Y., Tanaka, N., and Fujiwara, T. (2006) *In vivo* imaging of lymph node metastasis with telomerase-specific replication-selective adenovirus, *Nat. Med. 12*, 1213–1219.

26. Ghose, A. K., and Crippen, G. M. (1987) Atomic physicochemical parameters for three-dimensional-structure-directed quantitative structure-activity relationships. 2. Modeling dispersive and hydrophobic interactions, *J. Chem. Inf. Comput. Sci. 27*, 21–35.